

Dual-lobe reconnection and cusp-aligned auroral arcs

Milan Stephen E.¹, Bower Gemma E.¹, Carter Jennifer Alyson¹, Paxton Larry J.²,
Anderson Brian J.³, and Hairston Marc R.⁴

¹University of Leicester

²Johns Hopkins University

³John Hopkins Univ.

⁴University of Texas at Dallas

November 16, 2022

Abstract

Following the St. Patrick's Day (17 March) geomagnetic storm of 2013, the interplanetary magnetic field had near-zero clock angle for almost two days. Throughout this period multiple cusp-aligned auroral arcs formed in the polar regions; we present observations of, and provide a new explanation for, this poorly-understood phenomenon. The arcs were observed by auroral imagers onboard satellites of the Defense Meteorological Satellite Program (DMSP). Ionospheric flow measurements and observations of energetic particles from the same satellites show that the arcs were produced by inverted-V precipitation associated with upward field-aligned currents at shears in the convection pattern. The large-scale convection pattern revealed by the Super Dual Auroral Radar Network (SuperDARN) and the corresponding FAC pattern observed by the Active Magnetosphere and Planetary Electrodynamics Response Experiment (AMPERE) suggest that dual-lobe reconnection was ongoing to produce significant closure of the magnetosphere. However, we propose that once the magnetosphere became nearly closed complicated lobe reconnection geometries arose that produced interleaving of regions of open and closed magnetic flux and spatial and temporal structure in the convection pattern that evolved on timescales shorter than the orbital period of the DMSP spacecraft.

Dual-lobe reconnection and cusp-aligned auroral arcs

S. E. Milan^{1,2*}, G. E. Bower¹, J. A. Carter¹, L. J. Paxton³, B. J. Anderson³,
and M. R. Hairston⁴

¹School of Physics and Astronomy, University of Leicester, Leicester, UK.

²Birkeland Centre for Space Sciences, University of Bergen, Norway.

³Johns Hopkins University Applied Physics Laboratory, USA.

⁴William B. Hanson Center for Space Sciences, University of Texas at Dallas, USA.

Key Points:

- Cusp-aligned arcs were observed for two days of near-zero clock angle IMF following the St. Patrick's Day storm of 2013
- Arcs were associated with upwards field-aligned currents associated with vorticity within a highly structured ionospheric convection pattern
- We propose that the magnetosphere was nearly closed, but complicated lobe reconnection geometries interleaved open and closed flux

*Department of Physics and Astronomy, University of Leicester, Leicester LE1 7RH, UK

Corresponding author: Steve Milan, steve.milan@le.ac.uk

Abstract

Following the St. Patrick's Day (17 March) geomagnetic storm of 2013, the interplanetary magnetic field had near-zero clock angle for almost two days. Throughout this period multiple cusp-aligned auroral arcs formed in the polar regions; we present observations of, and provide a new explanation for, this poorly-understood phenomenon. The arcs were observed by auroral imagers onboard satellites of the Defense Meteorological Satellite Program (DMSP). Ionospheric flow measurements and observations of energetic particles from the same satellites show that the arcs were produced by inverted-V precipitation associated with upward field-aligned currents at shears in the convection pattern. The large-scale convection pattern revealed by the Super Dual Auroral Radar Network (SuperDARN) and the corresponding FAC pattern observed by the Active Magnetosphere and Planetary Electrodynamics Response Experiment (AMPERE) suggest that dual-lobe reconnection was ongoing to produce significant closure of the magnetosphere. However, we propose that once the magnetosphere became nearly closed complicated lobe reconnection geometries arose that produced interleaving of regions of open and closed magnetic flux and spatial and temporal structure in the convection pattern that evolved on timescales shorter than the orbital period of the DMSP spacecraft.

Plain Language Summary

The geomagnetic storm that occurred on St. Patrick's Day in 2013 was followed by a period of almost two days during which the magnetic field embedded within the solar wind was pointing purely northwards, a rare occurrence. Auroral observations reveal that a series of auroral arcs formed near the geomagnetic poles which were aligned along the sunwards direction. Measurements of flows within the polar ionosphere reveal that these arcs were associated with shears in the convection pattern and electrical currents linking the magnetosphere and ionosphere. We propose a mechanism by which these flows could be produced, invoking complicated patterns of magnetic reconnection occurring at high latitudes on the dayside magnetopause. These observations shed light on the poorly-understood solar wind-magnetosphere-ionosphere coupling processes that occur when the interplanetary magnetic field is directed northwards.

1 Introduction

Milan et al. (2020) recently proposed that dual-lobe reconnection (DLR), occurring during periods of prolonged northwards interplanetary magnetic field (IMF), can close significant amounts of the previously open magnetic flux of the magnetosphere. This newly-closed flux is distributed to high latitudes in the dawn and dusk sectors, producing the horse-collar auroras (HCA) morphology and giving the polar cap a teardrop shape (e.g., Murphree et al., 1982; Hones Jr et al., 1989; Elphinstone et al., 1993). In this paper we discuss what happens if this process continues until the magnetosphere approaches total closure and the role of DLR in producing the cusp-aligned auroral arcs that appear across the polar regions during northwards-directed IMF.

Dungey's open model of the magnetosphere (Dungey, 1961), invoking magnetic reconnection at the low latitude dayside magnetopause and in the magnetotail (Figure 1a), has been extremely successful for explaining many aspects of the structure and dynamics of the magnetosphere, including the excitation of magnetospheric and ionospheric convection (the typical twin-cell convection pattern), the dependence of geomagnetic activity on the orientation and strength of the IMF (Fairfield & Cahill Jr, 1966; Fairfield, 1967), the existence of an extended magnetotail (Wolfe et al., 1967; Ness et al., 1967) and regions near the poles largely devoid of auroras (the polar caps). The extension of Dungey's picture to include time-dependent dayside and nightside reconnection rates, the expanding/contracting polar cap model (Cowley & Lockwood, 1992), has allowed it to incorporate phenomena such as substorms (Lockwood & Cowley, 1992; Milan et al., 2007) and

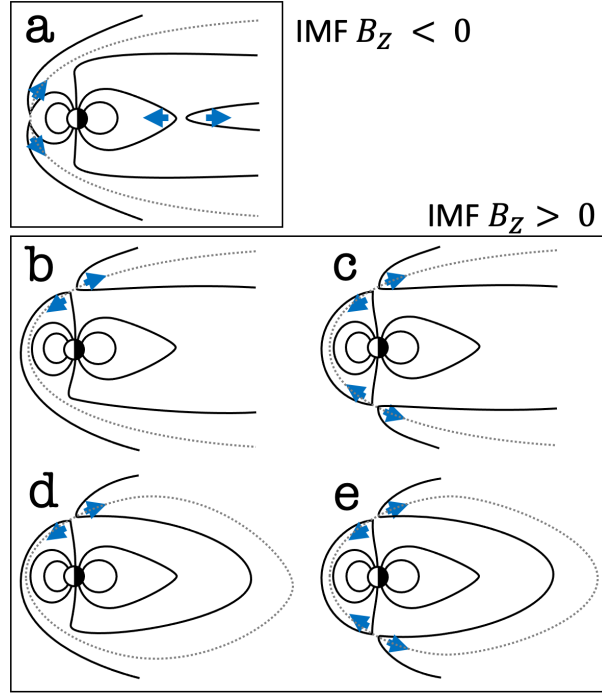


Figure 1. A schematic diagram of the reconnection geometries available for southward and northward IMF. (a) Southward IMF leading to reconnection of closed magnetic flux near the subsolar magnetopause, in turn leading to magnetotail reconnection, together driving the Dungey cycle. (b) Northward IMF and single lobe reconnection with open magnetic flux in the northern hemisphere; the open flux content of the magnetosphere is unchanged. (c) Dual lobe reconnection occurring with open lobe flux in both hemispheres; open flux is closed. (d) Single lobe reconnection in the northern hemisphere in a closed magnetosphere, opening magnetic flux. (e) Dual lobe reconnection in a closed magnetosphere; the magnetosphere remains closed. Adapted from Cowley (1981).

65 geomagnetic storms (Milan et al., 2009). Day- and nightside reconnection rates can also
 66 be used to assess the open flux content and length of the magnetotail (Milan, 2004).

67 During northwards IMF (or NBZ) conditions distorted convection, which can include
 68 sunward flows at noon, is observed within the polar ionosphere (e.g., Reiff & Burch,
 69 1985; Huang et al., 2000; Chisham et al., 2004), driven by the occurrence of recon-
 70 nection between the IMF and the magnetic field of the magnetospheric lobes, tailward of
 71 the cusps (Dungey, 1963; Cowley, 1981). If there is a significant IMF B_Y component then
 72 single lobe reconnection (SLR) occurs, that is an individual IMF field line reconnects in
 73 the northern or southern hemisphere only (Figure 1b). In this case an asymmetric pat-
 74 tern of flows is observed, the sunward flow having a significant dawnwards or duskwards
 75 component depending on the polarity of B_Y , produced by magnetic tension forces on the
 76 newly-reconnected field lines. Usually, SLR does not change the open magnetic flux con-
 77 tent of the magnetosphere, occurring with an open lobe field line and resulting in a new
 78 open field line. On the other hand, if $B_Y \approx 0$ then dual-lobe reconnection can occur,
 79 in which the same IMF field line reconnects in both hemispheres, producing closed field
 80 lines (Figure 1c). In this case a relatively symmetrical pattern of ionospheric flows is ex-
 81 pected, as discussed by Milan et al. (2020).

Under prolonged NBZ conditions the magnetotail can become unusually short (Fairfield et al., 1996) and display atypical structure and dynamics (e.g., Huang et al., 2002), suggesting that the magnetosphere is entirely closed. In this paper we discuss the possibility that this closure is caused by prolonged DLR. The role of DLR in producing partial flux closure has been investigated (Imber et al., 2006, 2007; Marcucci et al., 2008; Milan et al., 2020), but the process is still poorly understood. However, it has been asserted on the basis of magnetospheric simulations, that in the case of purely northward IMF DLR can close the magnetosphere entirely (Figure 1e) and magnetospheric circulation goes into reverse, with sunward ionospheric flows at noon and antisunward return flows at lower latitudes (Song et al., 1999; Siscoe et al., 2011). On the other hand, if SLR occurs in a closed magnetosphere, then flux will be reopened (Figure 1d). In this paper we discuss flux closure by DLR and the complicated dynamics that are driven when the magnetosphere is (nearly) closed.

Auroral dynamics help to shine light on the complicated processes that occur under NBZ conditions (Zhu et al., 1997; Kullen, 2012; Hosokawa et al., 2020; Fear, 2021). NBZ auroral features can include a cusp spot (Milan et al., 2000b; Frey et al., 2002; Carter et al., 2020), high latitude detached arcs or HiLDAs (Frey, 2007; Carter et al., 2018; Han et al., 2020), and transpolar arcs (e.g., Frank et al., 1982; Kullen et al., 2002; Cumnock et al., 2002; Cumnock & Blomberg, 2004; Milan et al., 2005; Fear et al., 2014; Carter et al., 2017). Under purely NBZ conditions ($B_Y \approx 0$), when DLR is expected to occur, the polar regions can become filled with multiple sun-aligned arcs, also known as cusp-aligned arcs due to their characteristic pattern (Y. Zhang et al., 2016), which are as yet poorly understood (e.g., Q.-H. Zhang et al., 2020). As they form under similar conditions, we might expect that horse-collar auroras and cusp-aligned arcs are in some way related. In this paper we present observations of auroras, energetic particle precipitation, ionospheric flows, and field-aligned currents that support the suggestion that closure of the magnetosphere can occur through DLR, producing HCA, and that this is also related to the formation of cusp-aligned arcs.

2 Observations

We employ observations of the auroras, ionospheric flows, and precipitating particles in both northern and southern hemispheres (NH and SH) from the Defense Meteorological Satellite Program (DMSP) F16, F17, and F18 satellites in sun-synchronous orbits near an altitude of 850 km. The Ion Driftmeter (IDM) component of the Special Sensors–Ions, Electrons, and Scintillation thermal plasma analysis package or SSIES (Rich & Hairston, 1994) measured the cross-track ionospheric convection flow at 1 s cadence (approx. 7 km spatial resolution). The Special Sensor Ultraviolet Spectrographic Imager or SSUSI experiment (Paxton et al., 1992), measured auroral luminosity in a swath either side of the orbit in the Lyman-Birge-Hopfield short (LBHs) band, 140 to 150 nm (see Paxton and Zhang (2016); Paxton et al. (2017, 2021) and the references cited therein for further description of the instrument and data products). The Special Sensor for Precipitating Particles version 4 or SSJ/4 instrument (Hardy, 1984) provided measurements of precipitating ions and electrons between 30 eV and 30 keV, in 19 logarithmically-spaced energy steps, at a cadence of 1 s.

The Super Dual Auroral Radar Network or SuperDARN (Chisham et al., 2007) provided measurements of ionospheric flows in the NH. We also present observations of the NH and SH field-aligned currents (FACs) derived from magnetometer measurements onboard the satellites of the Iridium telecommunications constellation processed using the from the Active Magnetosphere and Planetary Electrodynamics Response Experiment (AMPERE) technique (Anderson et al., 2000; Waters et al., 2001; Coxon et al., 2018).

The interval of interest is 17 to 19 March 2013, inclusive, encompassing the St. Patrick’s Day storm of 2013. The IMF conditions, derived from the OMNI dataset (King & Pa-

133 pitashvili, 2005), which drove this storm are shown in panel (g) of Figure 2. A step in
 134 solar wind ram pressure arrived at Earth shortly before 06 UT on 17 March (not shown),
 135 accompanied by an enhancement in the IMF magnitude. The GSM B_Y and B_Z com-
 136 ponents of the IMF fluctuated until 15 UT; from 15 UT B_Z was consistently negative
 137 until approximately 00 UT on 18 March, producing the main phase of the storm. For
 138 the majority of the next 50 hours, B_Z was positive and B_Y near zero, such that the clock
 139 angle, $\theta = \text{atan2}(B_Y, B_Z)$, shown in panel (h), was close to 0° . Periods of small clock
 140 angle are highlighted by vertical lines, being 01 to 12 UT and 15 to 20 UT on 18 March,
 141 and 04 to 15 UT on 19 March; we will refer to these as intervals I, II, and III, respec-
 142 tively.

143 Panels (a) to (d) show “keograms” of auroral observations from the SSUSI instru-
 144 ments on DMSP F16 and F17 in the northern and southern hemispheres. These show
 145 the auroral emission in the LBHs band along the dawn-dusk meridian with a latitudi-
 146 nal resolution of 1° and a cadence of approximately 110 minutes (the orbital period of
 147 the spacecraft). Grey regions show missing data: either missing images, or portions of
 148 the dawn-dusk meridian that were not sampled (predominantly in the southern hemi-
 149 sphere). Panels (e) and (f) show corresponding keograms of field-aligned current mag-
 150 nitude (red and blue for upwards and downwards FACs, respectively) from AMPERE,
 151 with a latitudinal resolution of 1° and a cadence of 10 minutes.

152 Prior to interval I, pairs of upwards/downwards FACs seen at dawn and dusk are
 153 the region 1 and region 2 (R1/R2) currents first identified by Iijima and Potemra (1976).
 154 A good correspondence between the location of the FACs and auroras is seen. FACs and
 155 auroras are mainly located between colatitudes of 16° and 20° before the arrival of the
 156 shock, and between 20° and 35° during the storm main phase. The enlarged polar cap
 157 indicates that the open flux content of the magnetosphere, F_{PC} , was enhanced during
 158 the period of strong driving. From the start of interval I until 19 UT on 19 March the
 159 auroras and FACs contracted polewards, being mainly located polewards of 18° colat-
 160 itude, and were weak. The FACs were no longer R1/R2 currents (which are associated
 161 with convection during southward IMF (Milan, 2013; Milan et al., 2017)), but as will be
 162 discussed below were produced by dayside processes during NBZ. During intervals I and
 163 III, especially as observed by DMSP F16, the auroras extended all the way to the poles
 164 such that the polar cap disappeared, and indeed later we will argue that the magneto-
 165 sphere was probably nearly closed at these times. At the end of the interval, after 20 UT
 166 on 19 March, the IMF rotated southwards, the R1/R2 FACs reappeared and the auro-
 167 ras and FACs progressively expanded to lower latitudes, with an open polar cap.

168 Tick marks and letters at the top of Figure 2 refer to panels of Figure 3, which show
 169 the auroras observed in the LBHs band by the SSUSI instrument during passes of DMSP
 170 F16, F17, and F18 over the northern and southern hemispheres. Noon is to the top and
 171 dawn to the right of each panel. Grey circles show lines of magnetic latitude in steps of
 172 10° ; note that all panels are on the same grid, expect panel (b) which extends to lower
 173 latitudes as this occurs during the main phase of the storm. Superimposed on each panel
 174 is the cross-track component of the ionospheric flow as measured by the ion driftmeter
 175 (IDM), with a scale shown in panel (a). The dial in each panel shows the concurrent IMF
 176 vector in the $B_Y - B_Z$ plane, the radius of the circle representing a magnitude of 10 nT.

177 Panel (a) is from the period prior to the shock arrival and shows a typical auro-
 178 ral oval configuration with an empty polar cap; the spacecraft track is too far towards
 179 the dayside to unambiguously identify the ionospheric flow pattern, but the observed flows
 180 are consistent with a standard twin-cell convection pattern. Panel (b) is from the main
 181 phase of the storm, and shows bright auroras expanded to low latitudes, an enlarged po-
 182 lar cap, and strong twin-cell convection.

183 Panels (c), (d), and (e) are from the beginning of interval I, when the IMF has clock
 184 angles $|\theta| < 20^\circ$ and dual lobe reconnection might be expected to occur. Unfortunately,

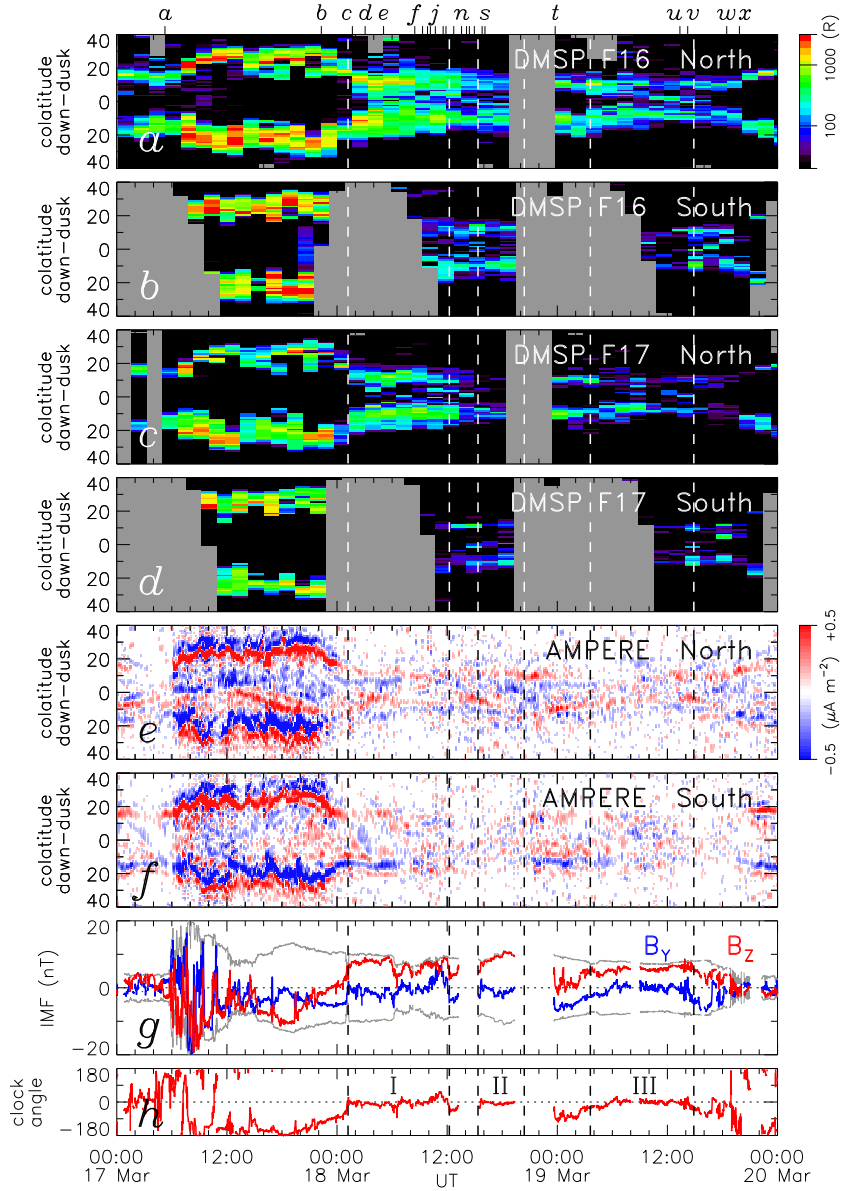


Figure 2. Observations of auroras, field-aligned currents, and interplanetary magnetic field for three days, 17 to 19 March 2013. (a) to (d) Auroral observations along the dawn-dusk meridian in the northern and southern hemispheres from the SSUSI instruments on DMSP F16 and F17. (e) and (f) AMPERE observations of field-aligned current density along the dawn-dusk meridian in the northern and southern hemispheres. Red and blue shading indicate upwards and downwards FACs, respectively. (g) IMF B_y (blue) and B_z (red) components, and total IMF field strength (grey). (h) IMF clock angle. Three periods of near-zero clock angle, labelled I, II, and III, are indicated by vertical dashed lines. Tick marks at the top correspond to panels in Figure 3.

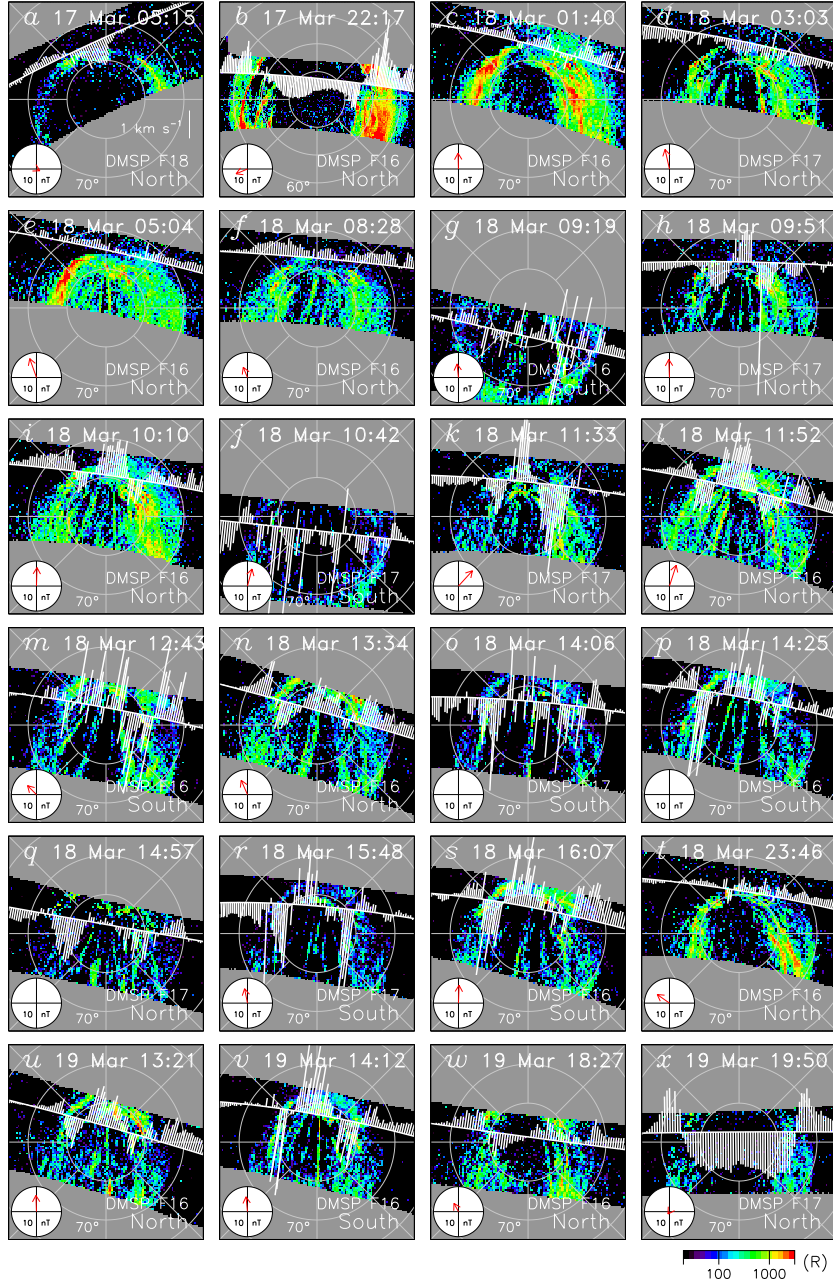


Figure 3. Observations of the auroral emission made by the SSUSI instruments onboard DMSP F16, F17, and F18 on 17 to 19 March 2013 on a geomagnetic latitude and local time grid, with noon towards the top. Circles indicate latitudes of 60, 70, and 80°; note all panels are on the same scale, except (b) which extends to lower latitudes. Superimposed on each panel are cross-track ionospheric flow vectors from the IDM instrument on DMSP, with the scale indicated in panel (a). The dial plots show the IMF B_Y and B_Z components (when available), with the circumference of the circle representing 10 nT. For reference, 1 kR in the LBHs band corresponds approximately to an International Brightness Coefficient (IBC) class 1 visible aurora (Chamberlain, 1961), or $1 \text{ erg cm}^{-2} \text{ s}^{-1}$ ($1 \text{ J m}^{-2} \text{ s}^{-1}$).

185 the DMSP orbit is not able to confirm the convection pattern during this period (though
 186 this will be discussed further below). However, the auroral evolution at this time is con-
 187 sistent with the DLR scenario described by Milan et al. (2020): in panel (c) the auro-
 188 ras have contracted to high latitudes, but a clear polar cap is still observed; in panel (d)
 189 cusp-aligned arcs appear poleward of the dawn and dusk sectors of the auroral oval; and
 190 in panel (e) the polar regions are filled with auroras, with the appearance of multiple cusp-
 191 aligned arcs. Milan et al. (2020) interpreted similar observations as the closure of open
 192 flux by DLR, producing sunward ionospheric flows across the noon sector polar bound-
 193 ary, and the distribution of this newly-closed flux to the high-latitude dawn and dusk
 194 sectors by antisunwards flows; however, in this example that process has continued and
 195 the whole polar regions have filled with auroras. Prior to DLR the open field lines are
 196 evacuated of plasma, so the polar cap is largely devoid of auroras; however, the newly-
 197 closed flux is expected to be laden with captured solar wind plasma, which could give
 198 rise to the auroral emission seen at high latitudes.

199 Most other panels in Figure 3 show that the polar regions were filled with cusp-
 200 aligned arcs for the majority of the time until the end of interval III. Here we will de-
 201 scribe just a few particular examples and return to others in the Discussion. From pan-
 202 els (h) to (v) the orbits of the spacecraft allow the dayside convection pattern to be mea-
 203 sured, and confirm the flows expected for DLR, that is, sunward near noon and antisun-
 204 ward flows into the high-latitude dawn and dusk sectors, and sometimes sunward flows
 205 at latitudes below the main auroral emission.

206 Panels (t) and (w) show periods when the IMF has rotated to $|\theta| \sim 45^\circ$, when
 207 DLR is no longer expected but single lobe reconnection (SLR) will open flux (see Dis-
 208 cussion) and produce lobe stirring. In both cases the polar regions become devoid of au-
 209 roras suggesting an open polar cap. In the case of panel (w), the ionospheric flows con-
 210 firm the expected convection pattern for SLR. Between these times, panels (u) and (v)
 211 show that when the IMF returns to low clock angles the flow pattern becomes consis-
 212 tent with DLR again, and the polar cap refills with auroras in both the northern and south-
 213 ern hemispheres.

214 In panel (x) the IMF has rotated to become southwards, the convection pattern
 215 becomes twin-celled and the polar cap is open, consistent with the observations at this
 216 time in Figure 2.

217 Figure 4 shows AMPERE-derived field-aligned current density, in both the north-
 218 ern and southern hemispheres, at four selected times. At each time, especially in the north-
 219 ern hemisphere, the FACs are consistent with DLR and the vorticity of the associated
 220 convection pattern (often referred to as NBZ FACs). Reverse, lobe cells are expected to
 221 be accompanied by a pair of up/down FACs straddling noon at latitudes near or above
 222 80° , with reversed-polarity FACs at lower latitudes, as discussed by Milan et al. (2020).
 223 Such a pattern is observed in all panels (except the SH in panel (a)), but the strength
 224 of the FACs is greatest in the northern hemisphere. The strength of NBZ FACs is an-
 225 ticipated to be controlled by the conductance of the ionosphere (Milan et al., 2017), though
 226 it is not expected that there will be much hemispherical asymmetry in the conductance
 227 in these near-equinox observations. The location of the solar terminator (green) in each
 228 hemisphere suggests that the conductance will be somewhat higher in the northern hemi-
 229 sphere, except in panel (a).

230 Panel (b) indicates that the ionospheric flows measured by IDM are consistent with
 231 DLR flows. Concurrent SuperDARN measurements (right-most panel) show reverse twin-
 232 cell convection associated with the NBZ FACs and weak nightside flows which are gen-
 233 erally antisunwards along the midnight meridian with return flows at dawn and dusk,
 234 consistent with average flow patterns for purely northwards IMF (e.g., Thomas & Shep-
 235 herd, 2018). Panels (c) and (d) (corresponding to panels (u) and (v) in Figure 3) show
 236 that DLR flows of similar speeds are observed in both the NH and SH, despite the dif-

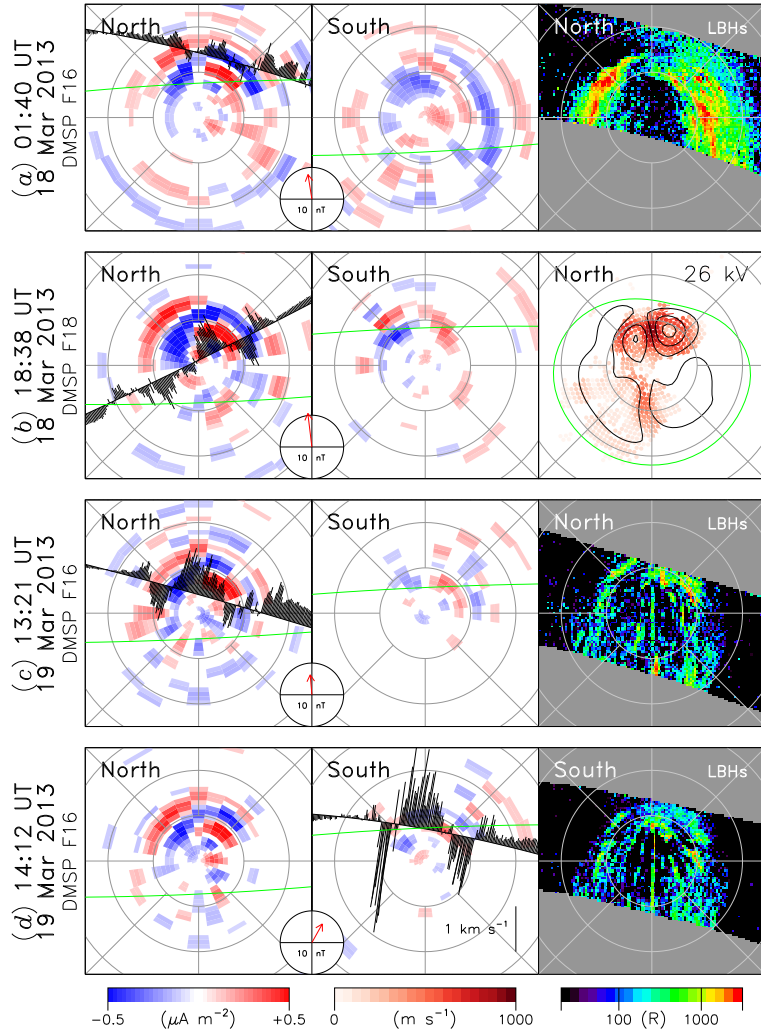


Figure 4. Left and middle panels show AMPERE observations of field-aligned current density in the northern and southern hemispheres at times of selected passes by DMSP. The data are presented on a geomagnetic latitude and local time grid, with noon at the top and circles representing latitudes of 60°, 70°, and 80°, with the solar terminator indicated in green. Cross-track ionospheric flow vectors from IDM are superimposed on the hemisphere in which the pass occurred; the scale is indicated in panel (d). The dial plots show the IMF B_Y and B_Z components. Right panels show the auroral emission measured by SSUSI (panels a, c, and d) or the ionospheric flow pattern inferred from SuperDARN observations (panel b); in the latter, the green circle is the low latitude extent of the convection pattern. In the latter case, the location of radar observations and the convection speed are indicated by shading; contours of electrostatic potential are indicated in steps of 6 kV.

237 ference in FAC magnitudes. The polar regions are filled with auroral forms in both NH
 238 and SH. That is, the flows and auroras resulting from DLR are highly symmetrical in
 239 the two hemispheres.

240 Panel (a) occurs at the start of interval I (and corresponds to Figure 3c), during
 241 the period that the horse-collar formation of auroras is first developing. Although ear-
 242 lier we could not confirm that DLR flows were occurring at this time, due to the orbit
 243 of the DMSP spacecraft, here we see that the DLR FAC pattern is indeed present. The
 244 DLR FACs in panel (a) are located at slightly lower latitudes than those in panels (c)
 245 and (d), as are the auroral emissions as a whole. This indicates that the presence of an
 246 open polar cap affects the location of the auroras and associated FAC patterns.

247 We now turn to an investigation of the particle signatures observed during four rep-
 248 resentative orbits of DMSP: Figure 5 in which the satellite track passes the sunward-most
 249 edge of the auroral emission, Figure 6 in which the spacecraft crosses the NBZ FACs,
 250 Figure 7 in which the track is antisunwards of the NBZ FACs, and Figure 8 in which the
 251 nightside is observed. All are presented in the same format. The AMPERE FACs in both
 252 NH and SH are shown at the top, with the IDM measurements superimposed on the hemi-
 253 sphere in which the pass occurred. In the next row, the SSUSI LBHs observations are
 254 shown twice, with the IDM measurements superimposed in the right-hand panel. The
 255 panels below these show measurements along the DMSP track as a function of time; in
 256 the case of SH passes the time axis is reversed so that in all cases the observations are
 257 presented with dusk at the left and dawn at the right. These panels show the SSUSI ra-
 258 diance intensity under the spacecraft, spectrograms of the precipitating electrons and
 259 ions from SSJ/4, the cross-track flow speed (V_{\perp} , positive sunwards) from IDM (also su-
 260 perimposed on the electron spectrogram), and the FAC magnitude (positive upwards)
 261 along the spacecraft track, derived from the AMPERE observations.

262 In Figure 5 (corresponding to Figure 3h), DMSP F17 passes at the sunward edge
 263 of the auroras. The DLR-driven flow pattern is very clear in the IDM measurements, with
 264 little small-scale structure superimposed on the the antisunwards / sunwards / antisun-
 265 wards convection. At lower latitudes, hot electrons (up to and exceeding 10 keV) are ob-
 266 served, the signature of trapped plasma on closed field lines produced during the nor-
 267 mal Dungey cycle. Polewards of this are intense low energy (up to 1-2 keV) electrons and
 268 ions with a broad range of energies; the highest fluxes of ions are observed in the region
 269 of sunward flow. We interpret these ions and electrons as magnetosheath plasma pre-
 270 cipitating downstream of the lobe reconnection site (i.e., sunwards of the ionospheric pro-
 271 jection of the x-line). If we could observe the particle characteristics along the noon merid-
 272 ian we would expect a reverse dispersed ion signature within the sunward convection throat
 273 (Woch & Lundin, 1992).

274 We note an increase in electron energies observed at 09:51 UT, at the duskward
 275 edge of the convection pattern. In this region there is a negative gradient in V_{\perp} , which
 276 implies converging electric field and hence upward FAC, consistent with the AMPERE
 277 measurements. We interpret this as a region in which electrons are accelerated down-
 278 wards to carry the required FAC, producing a region of auroral emission near the 15 MLT
 279 meridian (arrow labelled 2). Examination of the panels in Figure 3 reveals that this blob
 280 of auroral emission is a consistent feature of the observations.

281 In Figure 6 (corresponding to Figure 3g), DMSP F17 passes further towards the
 282 pole and crosses the main region of NBZ FACs, with the down/up FAC pattern clearly
 283 observed in the bottom panel. The DLR flow pattern is again clear, but now there is more
 284 small-scale structure superimposed on the convection, with ± 500 m s⁻¹ flow variations
 285 seen around 13:04 and 13:08 UT. As F17 traverses from sunward to antisunward flow
 286 at 13:06 UT, a clear, broad inverted-V signature is seen in the electrons, co-located with
 287 a region of pre-noon auroral emission (arrow labelled 1); again, this auroral feature is
 288 consistently seen in Figure 3. Narrower inverted-V structures are seen to be associated

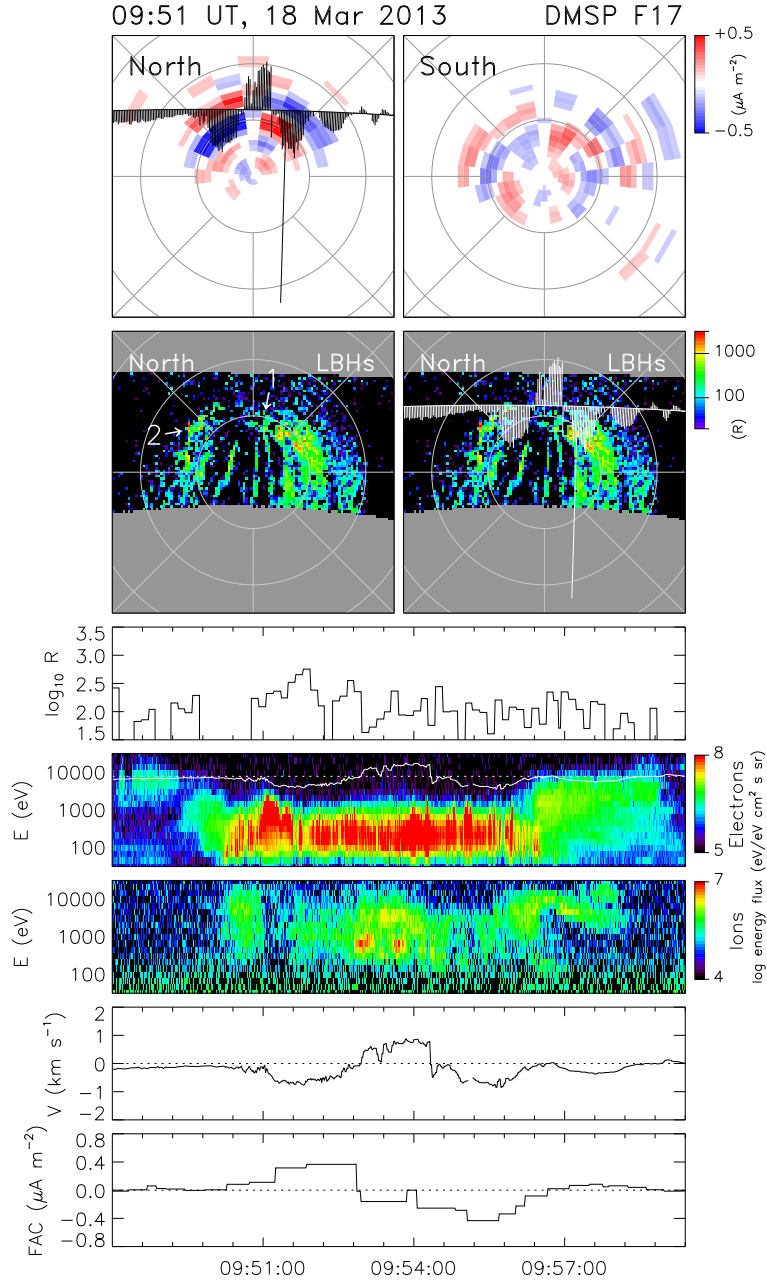


Figure 5. Observations from a pass of the northern hemisphere by DMSP F17 around 09:51 UT on 18 March 2013. Top panels show AMPERE observations of field-aligned current density in the northern and southern hemispheres at the time of the pass (averaged over the duration of the pass), presented on a geomagnetic latitude and local time grid with noon at the top. Circles indicate geomagnetic latitudes of 60, 70, and 80°. Ionospheric flow vectors from IDM are superimposed on the hemisphere in which the pass occurred. Below this, on the same grid, and auroral observations from SSUSI, presented twice, once with and once without the flow vectors superimposed. Arrows indicate type 1 and 2 HiLDAs (see text for details). The five panels below show parameters along the spacecraft track, over the duration of the pass. These are: auroral emission intensity from SSUSI, precipitating electron and ion spectrograms from the SSJ/4 instrument, the speed of the cross-track flow (positive sunwards) from IDM (also shown on the electro spectrogram), and the field-aligned current density from AMPERE.

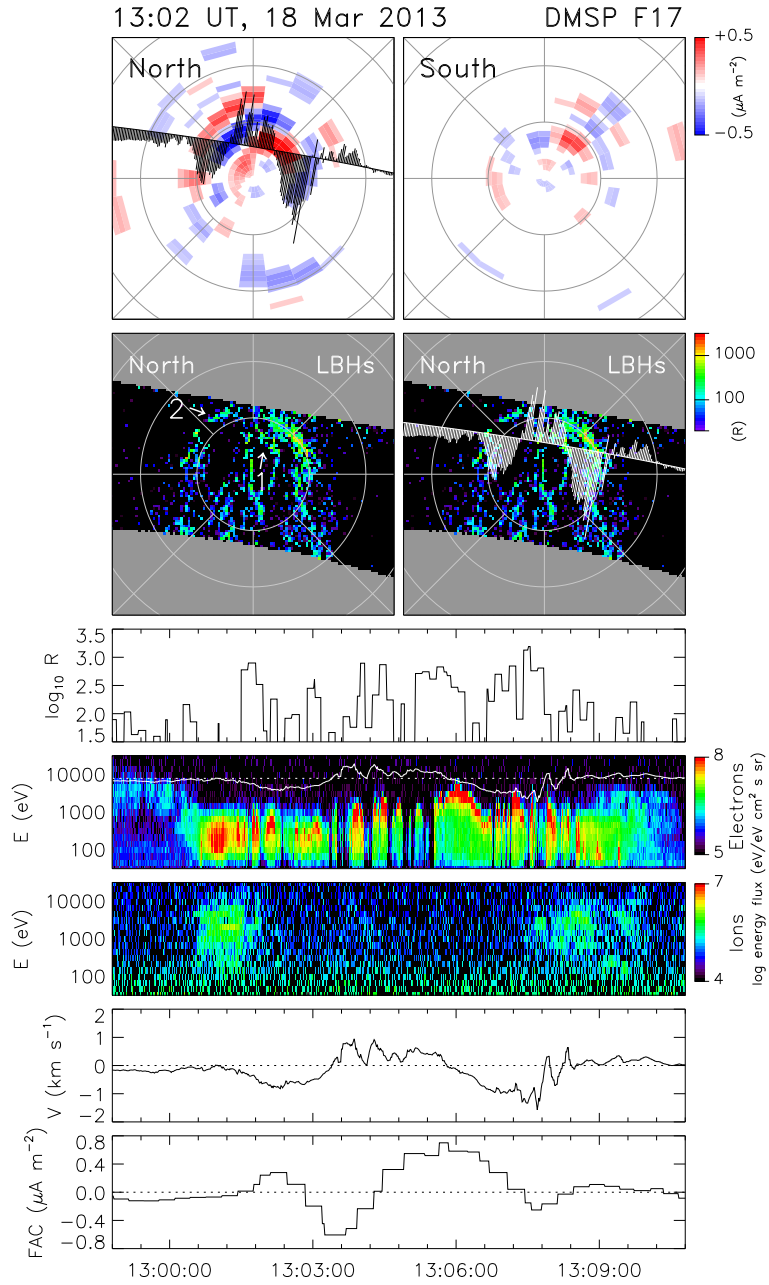


Figure 6. Similar to Figure 5, for the northern hemisphere pass of DMSP F17 around 13:02 UT on 18 March 2013.

289 with negative gradients in V_{\perp} where the small-scale but large-amplitude fluctuations are
 290 seen, both within the sunward flow region and the dawnside antisunward flow region.

291 The pre-noon auroral blob (1) associated with upward FAC identified in Figure 5
 292 is the high-latitude detached arc (HiLDA) discussed in a case study by Frey (2007) and
 293 statistically by Carter et al. (2018). HiLDAs are produced by the upward FAC associ-
 294 ated with the clockwise vorticity of the NBZ reverse convection pattern. Re-examination
 295 of the observations presented by Carter et al. (2018) reveals that on average a post-noon
 296 auroral blob is also observed co-located with the region 1 polarity FAC, similar to the
 297 post-noon auroral blob (2) identified in Figure 5. Both are produced by precipitation as-
 298 sociated with upward FAC due to the vorticity of the convection pattern, and the same
 299 morphology is observed in both NH and SH. Going forwards, we will refer to these as
 300 type 1 and 2 HiLDAs.

301 The pass of F16 in Figure 7 is similar to that in Figure 5, though crosses the noon
 302 meridian slightly antisunwards of the type 1 HiLDA. We show this pass to emphasise
 303 the consistency of the type 1 and 2 HiLDAs morphology. We also use it to highlight the
 304 multiple cusp-aligned arcs and associated flow-shears and inverted-V structures point-
 305 ing into the cusp region and even merging with the type 1 HiLDA, that is, reaching into
 306 the centre of the pre-noon DLR flow vortex. This pass also shows that the cusp-aligned
 307 arcs sunwards and antisunwards of the dawn-dusk meridian do not necessarily connect
 308 with each other, though this is discussed further below. Patches of ion precipitation are
 309 seen across the polar regions, suggesting that significant regions of closed flux exist.

310 In Figure 8, F16 passes antisunwards of the pole, crossing several prominent cusp-
 311 aligned arcs. The flows are highly structured, with multiple narrow sunward / antisun-
 312 ward flow shears with amplitudes in excess of $\pm 1 \text{ km s}^{-1}$. Negative gradients in V_{\perp} are
 313 associated with inverted-V signatures and colocated cusp-aligned arcs. These signatures
 314 are highly reminiscent of the observations reported by Q.-H. Zhang et al. (2020). Ion pre-
 315 cipitation is observed across most of the polar traversal, suggesting that the magnetic
 316 flux is closed; a relatively narrow region is devoid of ions between the two main cusp-
 317 aligned arcs, which might be interpreted as the poleward edges of the dawn and dusk
 318 regions of the HCA, indicating that the central region of flux could be open. No clear
 319 FAC signatures are seen by AMPERE along the F16 track, probably as a consequence
 320 of the relatively coarse spatial resolution of the observations.

321 Figure 9 (corresponding to Figure 3m) shows superimposed observations from F16
 322 and F18 as they traverse the SH polar regions at almost exactly the same time, with F18
 323 and F16 sunward and antisunward of the pole. Once again the flows are highly struc-
 324 tured, with flow shears being colocated with inverted-V electron precipitation and cusp-
 325 aligned auroral arcs. F18 observes mostly sunward flows near the noon meridian, but with
 326 large perturbations superimposed. There is consistency between the flows observed in
 327 the dawn sector where the spacecraft pass close to each other, but it is difficult to dis-
 328 cern the how the patterns fit together at dusk. It is probable that the nature of the flows
 329 are ordered by the pattern of cusp-aligned arcs, but the convection is clearly complicated
 330 and presumably time-variable. Ion precipitation present along both spacecraft tracks,
 331 especially on the nightside, suggest that much of the polar magnetic flux is closed.

332 In Figure 10 we examine the SuperDARN observations in more detail. Four radars
 333 of the network – Rankin Inlet, Inuvik, Hankasalmi, and Pykvibaer – contribute most to
 334 the measurements, and the line-of-sight velocity derived from the backscatter observed
 335 by each are shown in the left-hand panels (separated into two panels to avoid overlap),
 336 at five selected times. When combined using the standard SuperDARN “map-potential”
 337 fitting procedure (Ruohoniemi & Baker, 1998), these measurements give rise to the con-
 338 vection pattern presented in Figure 4b. The central beam of the Rankin Inlet radar looks
 339 almost directly into the convection throat at noon, observing sunward flows up to 1.5
 340 km s^{-1} (towards the radar, blue); to either side antisunward flows (away, red) are seen,

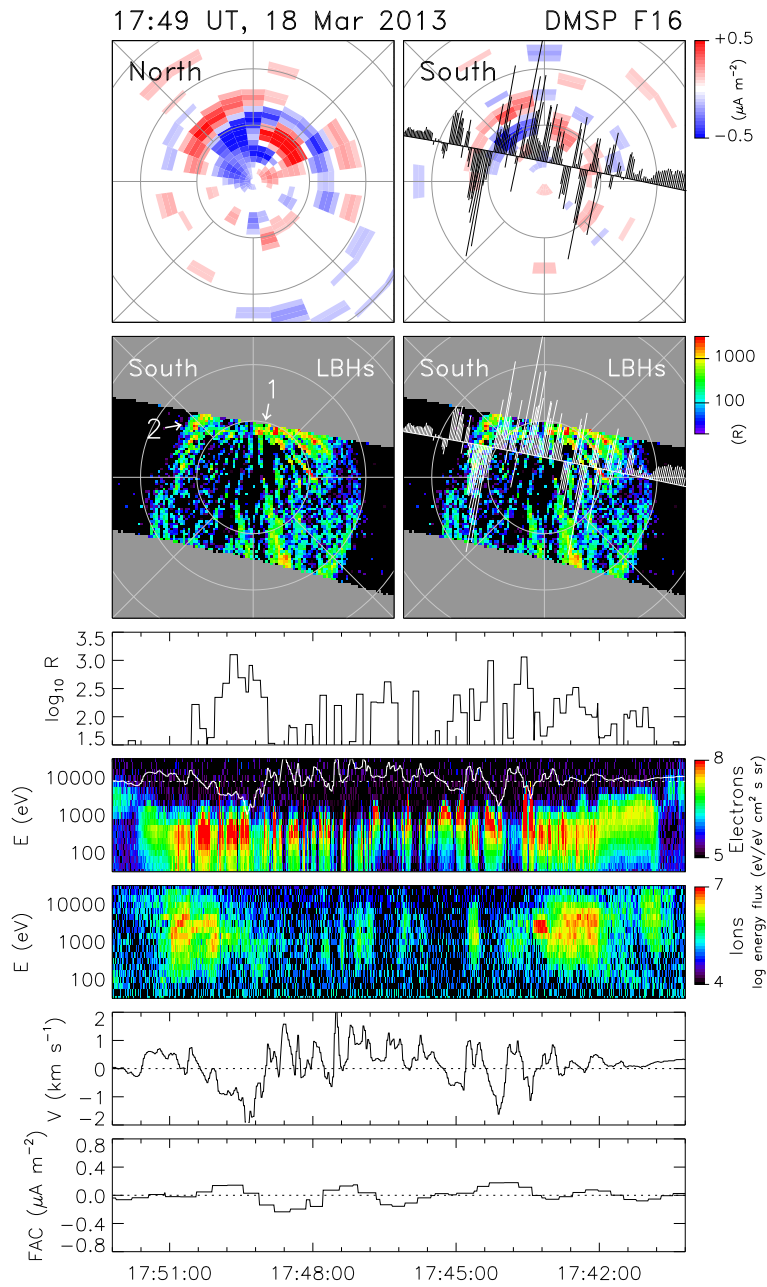


Figure 7. Similar to Figure 5, for the southern hemisphere pass of DMSP F16 around 17:49 UT on 18 March 2013. Note that for this pass of the southern hemisphere, the time axis has been reversed so that left and right correspond to dusk and dawn.

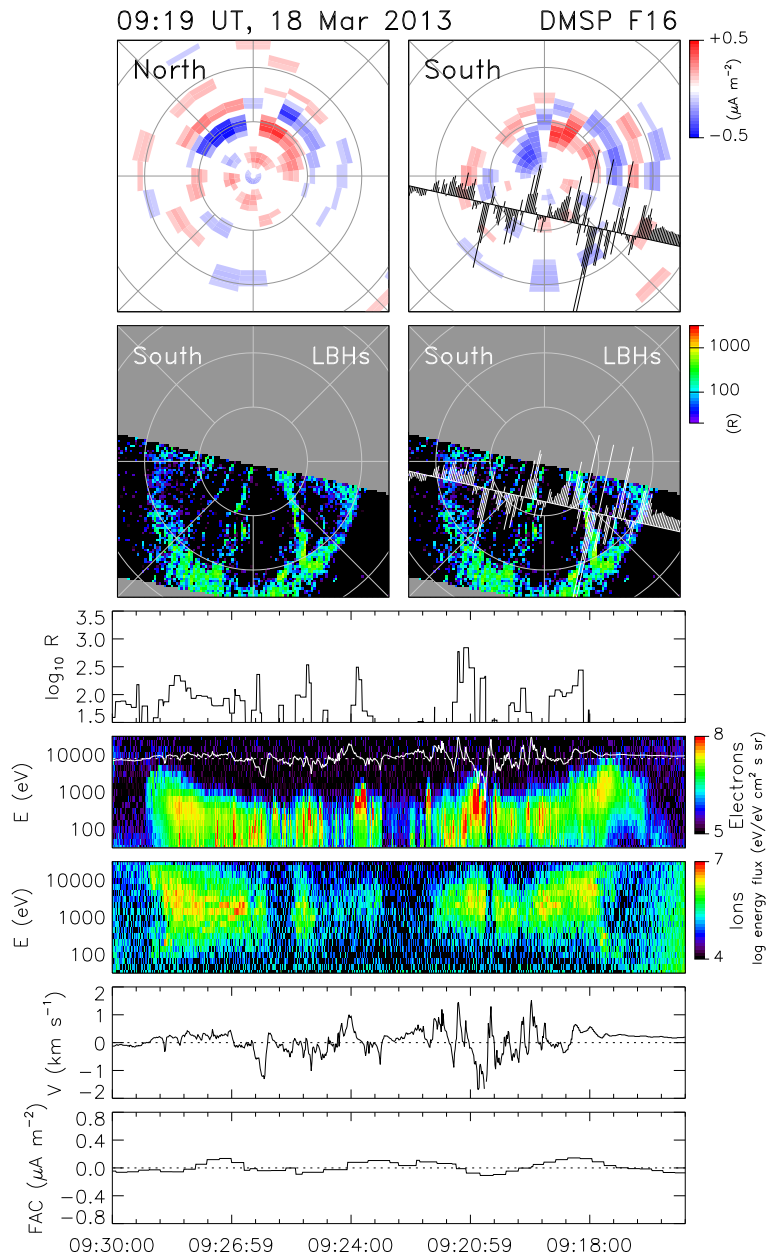


Figure 8. Similar to Figure 5, for the southern hemisphere pass of DMSP F16 around 09:19 UT on 18 March 2013. Note that for this pass of the southern hemisphere, the time axis has been reversed so that left and right correspond to dusk and dawn.

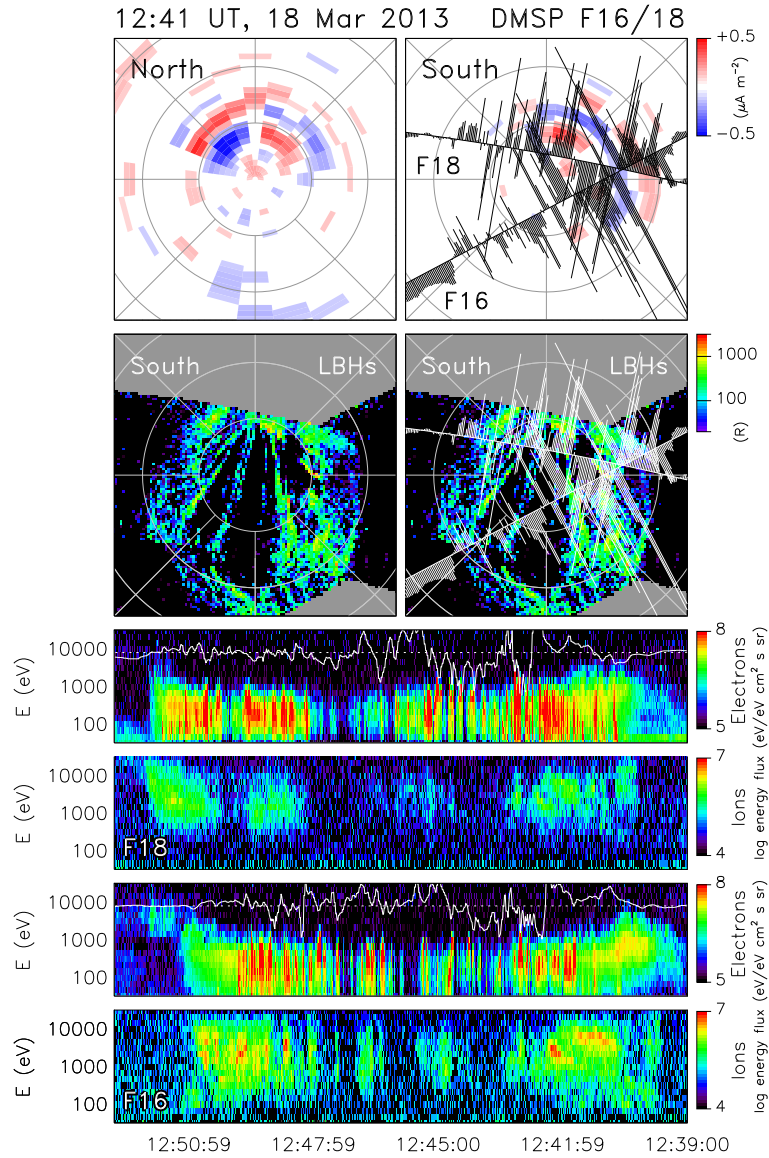


Figure 9. Observations from near-simultaneous passes of the southern hemisphere by DMSP F16 and F18 around 14:41 UT on 18 March 2013. The auroral observations from SSUSI on the two spacecraft have been superimposed. At the bottom, electron and ion spectrograms from SSJ/4 on the two spacecraft are shown, with ionospheric flows from IDM superimposed.

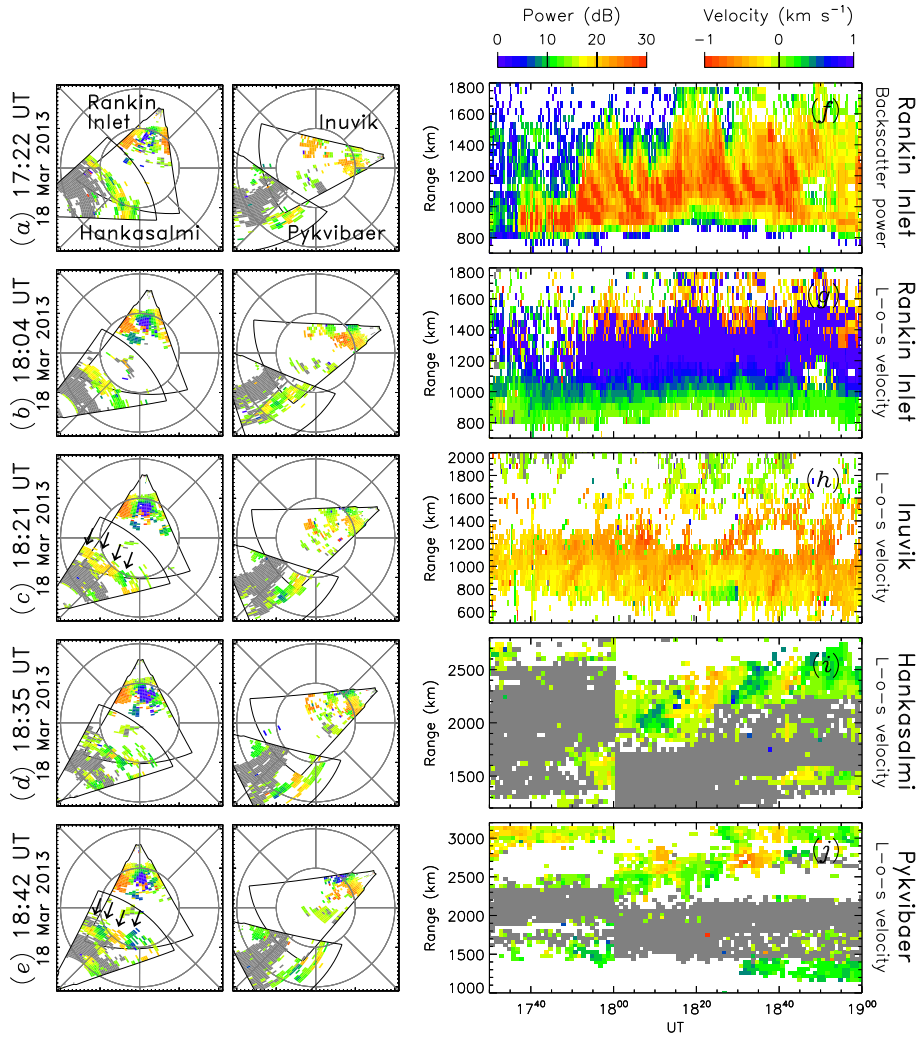


Figure 10. SuperDARN observations of northern hemisphere ionospheric flows between 17 and 19 UT on 18 March 2013, from the Rankin Inlet, Hankasalmi, Inuvik, and Pykkvibaer radars. On the left, measurements of line-of-sight flow speed (blue towards and red away from the radars) are presented on a geomagnetic latitude and local time grid, with noon at the top (in two separate panels to avoid overlap). To the right, range-time-parameter plots are presented of backscatter power from the Rankin Inlet radar, and line-of-sight flow speed for each of the four radars. In each case observations are shown from beam 6 of the radars, as these are roughly central beams, and because the Rankin Inlet and Inuvik radars were scanning this beam at a higher than usual temporal cadence (roughly 20 s as opposed to 2 min). Grey indicates echoes that have been classed as ground backscatter. Note that a change of operating frequency occurred at 18 UT at the Hankasalmi and Pykkvibaer radars.

341 consistent with the DLR convection pattern. This pattern of flows is observed by Rankin
 342 Inlet over the whole 1.5 h period shown, confirmed by the range-time-velocity panel (g).
 343 Flows are strongest and weakest at the farthest and nearest ranges, consistent with the
 344 rotation of the flow within the DLR throat region from sunwards to dawnwards and duskwards
 345 as latitude decreases. Panel (f) shows the corresponding range-time-power measurements.
 346 Regions of higher backscatter power are seen to quasi-periodically (3-6 min) propagate
 347 towards the radar; the curved nature of the striations suggests deceleration along the line-
 348 of-sight, consistent with the gradient in the velocity, and we suggest that regions of en-
 349 hanced backscatter power are entrained within the convection as it circulates within the
 350 DLR pattern. Although not obvious with the colour scale employed, these power enhance-
 351 ments are accompanied by fluctuations in the convection speed with an amplitude of sev-
 352 eral 100 m s^{-1} superimposed on the background $\sim 1 \text{ km s}^{-1}$ flow. The nature of these
 353 sunward-propagating power/velocity fluctuations is similar to poleward-moving radar
 354 auroral forms (PMRAFs) observed in the dayside polar cap during southward IMF, which
 355 are the counterpart of poleward-moving auroral forms (PMAFs) produced by flux trans-
 356 fer events (FTEs), that is quasi-periodic bursts of low latitude reconnection (e.g., Pin-
 357 nock et al., 1995; Provan et al., 1998; Milan et al., 2000a; Wild et al., 2001). The obser-
 358 vations of Figure 7 come from this interval. It is interesting to speculate if the time-variable
 359 flows observed by SuperDARN are associated with the cusp-aligned arcs observed to be
 360 reaching into the cusp region.

361 Flows on the nightside are monitored by the Hankasalmi and Pykvibaer radars. The
 362 fitted convection pattern, Figure 4b, shows relative weak and smooth flows on the night-
 363 side, in contradiction to the highly structured flows observed by DMSP IDM (Figures
 364 7 and 8). However, both nightside radars do observe towards/away line-of-sight veloc-
 365 ity enhancements with speeds of several 100 m s^{-1} (highlighted by arrows) that come
 366 and go and move about. The corresponding range-time-velocity panels, (i) and (j), show
 367 variations in the flow with periods close to 20 min. We conclude that structured flows
 368 are indeed observed by SuperDARN during this interval, but that the spatial resolution
 369 of the map-potential fitting procedure is too coarse to properly characterise this. The
 370 DMSP observations also imply that there are many small-scale FACs, accompanied in
 371 the case of upwards FACs by cusp-aligned arcs, but these are not resolved by the spa-
 372 tial resolution of the AMPERE technique.

373 **3 Discussion**

374 Following the main phase of the geomagnetic storm of St. Patrick's Day 2013, the
 375 IMF had near-zero clock angle for long periods over the next two days. Observations of
 376 auroral emissions, ionospheric flows, and field-aligned currents suggest that the magne-
 377 tosphere underwent dual-lobe reconnection, closing open magnetic flux (Dungey, 1963;
 378 Cowley, 1981). This lead first to a horse-collar auroral configuration (e.g., Murphree et
 379 al., 1982; Hones Jr et al., 1989; Elphinstone et al., 1993; Milan et al., 2020) before the
 380 whole polar regions became full of cusp-aligned auroral arcs. We interpret this as par-
 381 tial and then almost full closure of the magnetosphere. We anticipate that the poleward
 382 edge of the HCAs at dawn and dusk map to the magnetopause of the dawn and dusk
 383 flanks of the magnetosphere, encompassing the newly closed flux that is appended to the
 384 magnetosphere by DLR. If this process continued to full closure of the magnetosphere,
 385 we would expect that the dawn and dusk magnetopause would map to a line running
 386 along the noon-midnight meridian, and there are times when such an auroral arc is ob-
 387 served, for instance Figure 4 panels (c) and (d). If the magnetosphere does close entirely,
 388 then DLR should drive reverse convection (Song et al., 1999; Siscoe et al., 2011), and
 389 in general the observed flows support this. In addition, the observation of (presumably
 390 trapped) ion precipitation across most of the traversals of the polar regions by DMSP
 391 (Figures 7 and 8) suggest significant flux closure.

Figure 1 summarises the reconnection geometries available at the magnetopause for southward and northward IMF: (a) low latitude reconnection, (b) single lobe and (c) dual-lobe reconnection in an open magnetosphere, and (d) single lobe and (e) dual-lobe reconnection in a closed magnetosphere. Scenario (a) increases the open flux (the polar cap flux, F_{PC}) in the magnetosphere and drives the Dungey cycle, (b) neither increases nor decreases F_{PC} but produces lobe stirring, (c) reduces F_{PC} and causes reverse convection within the dayside polar regions. Scenario (d) opens flux, increasing F_{PC} , while (e) does not open flux but induces reverse convection throughout the outer magnetosphere and polar regions, as modelled by Song et al. (1999) and Siscoe et al. (2011).

For NBZ with near-zero IMF B_Y we expect first scenario (c) and then (e) to close the magnetosphere and then drive reverse convection within it. However, if B_Y becomes non-zero then (b) will halt the closure of the magnetosphere, and (d) will even reverse it. This is consistent with the disappearance of auroral emissions near the pole in Figure 3 panels (t) and (w). The southward turning of the IMF at the end of interval III, Figure 2, leads to low latitude reconnection which reopens the magnetosphere and drives Dungey cycle flows, as shown in Figure 3x. It is interesting to note that although the IMF magnitude is small (≈ 5 nT) and B_Z is only -1 nT at this time, the reopening of the magnetosphere is rapid and the strength of the flows is large. It appears that the magnetosphere “abhors a vacuum” and will reopen readily.

We anticipate that achieving full closure of the magnetosphere through DLR is difficult. As the magnetosphere approaches full closure, any IMF field line that reconnects in one hemisphere but not the other, as in scenario (d), will reopen flux. This failure to reconnect in both NH and SH could be caused by small variations in IMF B_Y , turbulence within the magnetosheath, or transient and/or episodic reconnection. It seems likely that during prolonged periods of near-zero clock angle, a complicated interleaving of regions of open and closed flux could be produced in the polar regions, with the magnetosphere nearly closed, but not entirely. Such bursty reconnection and the interleaving of open and closed flux could be related to the appearance of cusp-aligned arcs and fast flow channels, as discussed below.

That the magnetosphere is nearly closed explains why auroral emission can occur over the entire polar regions: the closed flux will contain plasma that can be accelerated to produce auroras; in contrast, the polar regions are usually devoid of auroras because the open lobes are evacuated. However, we have also shown that the auroral emission is not uniform, but comprises multiple cusp-aligned arcs. Although these arcs have been reported before (e.g., Q.-H. Zhang et al., 2020), their origin is still uncertain. Q.-H. Zhang et al. (2020) showed that such arcs are associated with inverted-V precipitation signatures and filamentary field-aligned currents, associated with shears in the convection flow, just as presented in this paper. They suggested that these convection shears were propagated into the central magnetotail by Kelvin-Helmholtz Instability (KHI) waves on the magnetopause. In their scenario it is necessary for the magnetosphere to be nearly closed, such that closed flux from the central tail maps across the polar regions where the arcs are observed: DLR can provide this closure. Also, if the arcs are formed by the KHI and waves propagating from the magnetopause towards the central tail, we might expect to see a “phase motion” of the arcs in the ionosphere. This phase motion would be expected to emanate from the noon-midnight meridian (where the dawn and dusk flank magnetopause would map if the magnetosphere was closed) and move to lower latitudes both dawnwards and duskwards. Unfortunately, the cadence of the SSUSI images is too coarse to allow this behaviour to be resolved.

Alternatively, we suggest that patchy and bursty lobe reconnection could also lead to flow channels. The interleaving of open and closed flux described above will lead to different reconnection geometries (as exemplified in Figure 1) at different points along the x-line. (See also the discussion in Fear et al. (2015) in the context of transpolar arcs.) The spatially and temporally structured ionospheric flows observed by the Rankin In-

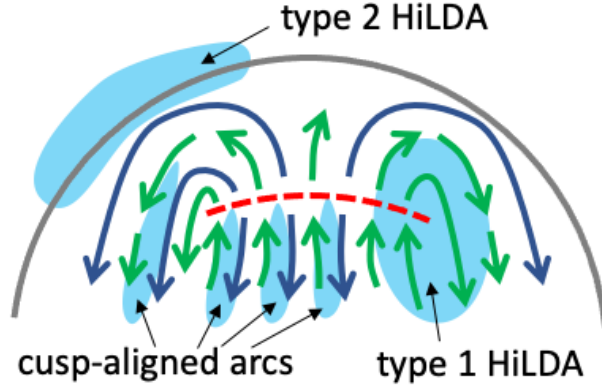


Figure 11. A schematic diagram of the ionospheric flows which could be driven by lobe reconnection in a magnetosphere that is nearly closed but has regions of open magnetic flux. The grey semicircle is the low latitude extent of the dayside convection pattern, with noon towards the top; the red dashed line is the ionospheric projection of the lobe reconnection x-line. Green and blue arrows show flow streamlines which might be driven for different reconnection geometries (see text for details). Blue shading indicates where vorticity in the flow will be associated with upwards field-aligned currents producing auroral emission, including type 1 and 2 HiLDAs (right and top-left) and cusp-aligned arcs.

445 let radar are indicative of bursty reconnection. A possible scenario is sketched in Fig-
 446 ure 11. The grey semicircle represents the low latitude extent of the dayside convec-
 447 tion pattern, and the red dashed line is the ionospheric projection of the lobe x-line. A com-
 448 plicated pattern of open and closed flux is envisaged across the polar regions. Portions
 449 of the x-line will be reconnecting in scenarios (b), (c), (d), or (e) from Figure 1, result-
 450 ing in either open or closed flux. In each case, sunward flow will be created sunward of
 451 the ionospheric projection of the x-line. However, in cases (b) and (d) the field line will
 452 be open and connected into the solar wind and will be subject to significant east-west
 453 magnetic tension forces; in cases (c) and (e) the field lines will be closed and draped across
 454 the dayside magnetopause, with little impetus to move. We might expect quite differ-
 455 ent evolutions of these differing field lines subsequent to reconnection. In all these cases
 456 however, the flows produced will be sunward on both the sunward and antisunward sides
 457 of the x-line, shown as green flow streamlines in Figure 11.

458 In Figure 1d we have envisaged that the single lobe reconnection occurs in the north-
 459 ern lobe, and the discussion above has applied to the northern hemisphere ionosphere.
 460 If, on the other hand, the reconnection occurs in the southern lobe, then in the north-
 461 ern hemisphere the field line will be opened but connected through the tail into the so-
 462 lar wind in the southern hemisphere. It is unclear how this field line will subsequently
 463 evolve, but certainly there is no immediate application of a tension force to make it move
 464 sunwards; we have shown possible antisunwards flows away from the x-line by blue stream-
 465 lines in Figure 11. We note that although the Rankin Inlet radar observes predominantly
 466 sunwards flows in the noon sector, at far ranges (around 1400 km in Figure 10), patches
 467 of antisunwards velocities are also seen: these could be the source of the antisunward flow
 468 channels seen by DMSP on the nightside, with the boundary between anti/sunwards flows
 469 seen by the radar mapping to the ionospheric projection of the x-line.

470 The result of the patchy and episodic reconnection will be bursty sunwards flows
 471 sunward of the x-line, with more complicated flows on the nightside, as suggested by the
 472 observations: it was for this reason that Figures 5 to 8 were shown in order of dayside

473 to nightside traversals of the polar regions by the DMSP spacecraft, with more uniform
 474 flows at the dayside and more complicated flows on the nightside. The schematic of Fig-
 475 ure 11 shows where vorticity in the convection pattern would give rise to upwards FACs
 476 and auroral emissions, including both type 1 and 2 HiLDAs and cusp-aligned arcs. We
 477 expect that this complicated pattern of flows would evolve with time, and indeed the flow
 478 channels and auroral arcs are seen to move about between passes of the DMSP space-
 479 craft. It is probable that the auroral emissions are even evolving during the spacecraft
 480 traversal of the polar regions (over approximately 20 mins), so the images should not be
 481 treated as a “snapshot” of the auroral pattern. There is some indication (e.g., Figure 7)
 482 that the dayside and nightside portions of the cusp-aligned arcs may not necessarily join,
 483 in which case they could be produced by different mechanisms, maybe the mechanism
 484 of Q.-H. Zhang et al. (2020) on the nightside and lobe reconnection on the dayside. On
 485 the other hand, this apparent disconnection could be a consequence of motions of the
 486 arcs during the traversal of DMSP. Higher temporal resolution auroral imaging would
 487 likely cast significant light on the formation and dynamics of the arcs.

488 **4 Conclusions**

489 We have reported the observation of cusp-aligned arcs during periods of near-zero
 490 IMF clock angle. Similarly to Q.-H. Zhang et al. (2020), we have shown that these arcs
 491 are associated with flow shears in the polar convection pattern. We propose that dual-
 492 lobe reconnection is first responsible for a significant closure of the magnetosphere, but
 493 subsequently complicated lobe reconnection geometries involving open and closed mag-
 494 netospheric field lines could produce these flow shears. This pattern would evolve with
 495 time, but highly similar patterns would be expected in the two hemispheres. We expect
 496 that high-cadence (minutes rather than 10s of minutes) imaging of the auroral emissions
 497 are required to fully resolve the formation mechanism of the arcs.

498 **Acknowledgments**

499 SEM and JAC are supported by the Science and Technology Facilities Council (STFC),
 500 UK, grant no. ST/S000429/1. GEB is supported by an STFC studentship. MRH was
 501 supported by the National Science Foundation under grant AGS-1929866 and by NASA
 502 under grant 80NSSC20K1071. The work at the Birkeland Centre for Space Science is sup-
 503 ported by the Research Council of Norway under contract 223252/F50. BH is supported
 504 by the Belgian National Fund for Scientific Research (FNRS). We acknowledge use of
 505 NASA/GSFC’s Space Physics Data Facility’s CDAWeb service (at [http://cdaweb.gsfc](http://cdaweb.gsfc.nasa.gov)
 506 [.nasa.gov](http://cdaweb.gsfc.nasa.gov)), and OMNI data. The OMNI data and the IMAGE WIC and SI12 data were
 507 obtained from CDAWeb (<https://cdaweb.gsfc.nasa.gov>). The DMSP/SSUSI file type
 508 EDR-AUR data were obtained from <http://ssusi.jhuapl.edu> (data version 0106, soft-
 509 ware version 7.0.0, calibration period version E0018). The DMSP/SSIES data were down-
 510 loaded from the Madrigal Database at Millstone Hill ([http://millstonehill.haystack](http://millstonehill.haystack.mit.edu)
 511 [.mit.edu](http://millstonehill.haystack.mit.edu)). The DMSP particle detectors were designed by Dave Hardy of AFRL, and
 512 data obtained from JHU/APL (<http://sd-www.jhuapl.edu/Aurora/>). AMPERE data
 513 were obtained from <http://ampere.jhuapl.edu>.

514 **References**

- 515 Anderson, B., Takahashi, K., & Toth, B. (2000). Sensing global Birkeland currents
 516 with Iridium® engineering magnetometer data. *Geophysical Research Letters*,
 517 *27*(24), 4045–4048. doi: <https://doi.org/10.1029/2000GL000094>
 518 Carter, J., Milan, S., Fear, R., Walach, M.-T., Harrison, Z., Paxton, L., & Hubert,
 519 B. (2017). Transpolar arcs observed simultaneously in both hemispheres.
 520 *Journal of Geophysical Research: Space Physics*, *122*(6), 6107–6120. doi:
 521 <https://doi.org/10.1002/2016JA023830>

- 522 Carter, J., Milan, S., Fogg, A., Paxton, L., & Anderson, B. (2018). The associa-
 523 tion of high-latitude dayside aurora with NBZ field-aligned currents. *Journal*
 524 *of Geophysical Research: Space Physics*, *123*(5), 3637–3645. doi: [https://doi](https://doi.org/10.1029/2017JA025082)
 525 [.org/10.1029/2017JA025082](https://doi.org/10.1029/2017JA025082)
- 526 Carter, J., Milan, S., Fogg, A., Sangha, H., Lester, M., Paxton, L., & Anderson,
 527 B. (2020). The evolution of long-duration cusp spot emission during lobe
 528 reconnection with respect to field-aligned currents. *Journal of Geophysical*
 529 *Research: Space Physics*, *125*, e2020JA027922. doi: [https://doi.org/10.1029/](https://doi.org/10.1029/2020JA027922)
 530 [2020JA027922](https://doi.org/10.1029/2020JA027922)
- 531 Chamberlain, J. (1961). *Physics of the aurora and airglow*. academic press, new york
 532 & london.
- 533 Chisham, G., Freeman, M., Coleman, I., Pinnock, M., Hairston, M., Lester, M., &
 534 Sofko, G. (2004). Measuring the dayside reconnection rate during an interval
 535 of due northward interplanetary magnetic field. *Annales Geophysicae*, *22*(12),
 536 4243–4258. doi: <https://doi.org/10.5194/angeo-22-4243-2004>
- 537 Chisham, G., Lester, M., Milan, S. E., Freeman, M., Bristow, W., Grocott, A., ...
 538 others (2007). A decade of the Super Dual Auroral Radar Network (Super-
 539 DARN): Scientific achievements, new techniques and future directions. *Surveys*
 540 *in Geophysics*, *28*(1), 33–109. doi: <https://doi.org/10.1007/s10712-007-9017-8>
- 541 Cowley, S. (1981). Magnetospheric and ionospheric flow and the interplanetary mag-
 542 netic field. *The Physical Basis of the Ionosphere in the Solar-Terrestrial Sys-*
 543 *tem, AGARD-CP-295*, (4-1)–(4-14).
- 544 Cowley, S., & Lockwood, M. (1992). Excitation and decay of solar wind-driven flows
 545 in the magnetosphere-ionosphere system. *Annales Geophysicae*, *10*, 103–115.
- 546 Coxon, J., Milan, S., & Anderson, B. (2018). A review of Birkeland current research
 547 using AMPERE. *Electric currents in geospace and beyond*, 257–278. doi:
 548 <https://doi.org/10.1002/9781119324522.ch16>
- 549 Cumnock, J., & Blomberg, L. (2004). Transpolar arc evolution and associated po-
 550 tential patterns. *Annales Geophysicae*, *22*(4), 1213–1231. doi: [https://doi.org/](https://doi.org/10.5194/angeo-22-1213-2004)
 551 [10.5194/angeo-22-1213-2004](https://doi.org/10.5194/angeo-22-1213-2004)
- 552 Cumnock, J., Sharber, J., Heelis, R., Blomberg, L. G., Germany, G., Spann, J., &
 553 Coley, W. (2002). Interplanetary magnetic field control of theta aurora devel-
 554 opment. *Journal of Geophysical Research: Space Physics*, *107*(A7), SIA–4. doi:
 555 <https://doi.org/10.1029/2001JA009126>
- 556 Dungey, J. (1961). Interplanetary magnetic field and the auroral zones. *Physical Re-*
 557 *view Letters*, *6*(2), 47.
- 558 Dungey, J. (1963). The structure of the exosphere, or adventures in velocity space.
 559 *Geophysics, The Earth's Environment*.
- 560 Elphinstone, R., Murphree, J., Hearn, D. J., Heikkila, W., Henderson, M., Cogger,
 561 L., & Sandahl, I. (1993). The auroral distribution and its mapping according
 562 to substorm phase. *Journal of atmospheric and terrestrial physics*, *55*(14),
 563 1741–1762.
- 564 Fairfield, D. (1967). Polar magnetic disturbances and the interplanetary magnetic
 565 field. *Space Research*, *VIII*, 107–119.
- 566 Fairfield, D., & Cahill Jr, L. (1966). Transition region magnetic field and polar mag-
 567 netic disturbances. *Journal of Geophysical Research*, *71*(1), 155–169.
- 568 Fairfield, D., Lepping, R., Frank, L., Ackerson, K., Paterson, W., Kokubun, S., ...
 569 Nakamura, M. (1996). Geotail observations of an unusual magnetotail under
 570 very northward IMF conditions. *Journal of Geomagnetism and Geoelectricity*,
 571 *48*(5), 473–487. doi: <https://doi.org/10.5636/jgg.48.473>
- 572 Fear, R. (2021). The northward IMF magnetosphere. *Magnetospheres in the Solar*
 573 *System*, 293–309. doi: <https://doi.org/10.1002/9781119815624.ch19>
- 574 Fear, R., Milan, S., Carter, J., & Maggiolo, R. (2015). The interaction between
 575 transpolar arcs and cusp spots. *Geophysical Research Letters*, *42*(22), 9685–
 576 9693. doi: <https://doi.org/10.1002/2015GL066194>

- 577 Fear, R., Milan, S., Maggiolo, R., Fazakerley, A., Dandouras, I., & Mende, S. (2014).
 578 Direct observation of closed magnetic flux trapped in the high-latitude mag-
 579 netosphere. *Science*, *346*(6216), 1506–1510. doi: [https://doi.org/10.1126/](https://doi.org/10.1126/science.1257377)
 580 [science.1257377](https://doi.org/10.1126/science.1257377)
- 581 Frank, L., Craven, J., Burch, J., & Winningham, J. (1982). Polar views of the
 582 Earth’s aurora with Dynamics Explorer. *Geophysical Research Letters*, *9*(9),
 583 1001–1004. doi: <https://doi.org/10.1029/GL009i009p01001>
- 584 Frey, H. (2007). Localized aurora beyond the auroral oval. *Reviews of Geophysics*,
 585 *45*(1). doi: <https://doi.org/10.1029/2005RG000174>
- 586 Frey, H., Mende, S., Immel, T., Fuselier, S., Clafin, E., Gérard, J.-C., & Hubert, B.
 587 (2002). Proton aurora in the cusp. *Journal of Geophysical Research: Space*
 588 *Physics*, *107*(A7), SMP–2. doi: <https://doi.org/10.1029/2001JA900161>
- 589 Han, D.-S., Feng, H.-T., Zhang, H., Zhou, S., & Zhang, Y. (2020). A new type
 590 of polar cap arc observed in the 1500 MLT sector: 1. Northern Hemisphere
 591 observations. *Geophysical Research Letters*, *47*(20), e2020GL090261. doi:
 592 <https://doi.org/10.1029/2020GL090261>
- 593 Hardy, D. A. (1984). Precipitating electron and ion detectors (SSJ/4) for the block
 594 5D/flights 6-10 DMSP satellites: Calibration and data presentation. *Rep.*
 595 *AFGL-TR-84-0317*.
- 596 Hones Jr, E., Craven, J., Frank, L., Evans, D., & Newell, P. (1989). The horse-collar
 597 aurora: A frequent pattern of the aurora in quiet times. *Geophysical Research*
 598 *Letters*, *16*(1), 37–40. doi: <https://doi.org/10.1029/GL016i001p00037>
- 599 Hosokawa, K., Kullen, A., Milan, S., Reidy, J., Zou, Y., Frey, H. U., . . . Fear, R.
 600 (2020). Aurora in the polar cap: A review. *Space Science Reviews*, *216*(1), 15.
 601 doi: <https://doi.org/10.1007/s11214-020-0637-3>
- 602 Huang, C.-S., Foster, J., Song, P., Sofko, G., Frank, L., & Paterson, W. (2002).
 603 Geotail observations of magnetospheric midtail during an extended period
 604 of strongly northward interplanetary magnetic field. *Geophysical Research*
 605 *Letters*, *29*(4), 15–1. doi: <https://doi.org/10.1029/2001GL014170>
- 606 Huang, C.-S., Sofko, G., Koustov, A., Andre, D., Ruohoniemi, J., Greenwald,
 607 R., & Hairston, M. (2000). Evolution of ionospheric multicell convection
 608 during northward interplanetary magnetic field with $|B_z/B_y| > 1$. *Jour-*
 609 *nal of Geophysical Research: Space Physics*, *105*(A12), 27095–27107. doi:
 610 <https://doi.org/10.1029/2000JA000163>
- 611 Iijima, T., & Potemra, T. (1976). The amplitude distribution of field-aligned cur-
 612 rents at northern high latitudes observed by Triad. *Journal of Geophysical Re-*
 613 *search*, *81*(13), 2165–2174. doi: <https://doi.org/10.1029/JA081i013p02165>
- 614 Imber, S., Milan, S., & Hubert, B. (2006). The auroral and ionospheric flow signa-
 615 tures of dual lobe reconnection. *Annales Geophysicae*, *24*(11), 3115–3129. doi:
 616 <https://doi.org/10.5194/angeo-24-3115-2006>
- 617 Imber, S., Milan, S., & Hubert, B. (2007). Observations of significant flux closure by
 618 dual lobe reconnection. *Annales Geophysicae*, *25*, 1617–1627. doi: [https://doi](https://doi.org/10.5194/angeo-25-1617-2007)
 619 [.org/10.5194/angeo-25-1617-2007](https://doi.org/10.5194/angeo-25-1617-2007)
- 620 King, J., & Papitashvili, N. (2005). Solar wind spatial scales in and comparisons
 621 of hourly Wind and ACE plasma and magnetic field data. *Journal of Geo-*
 622 *physical Research: Space Physics*, *110*(A2). doi: [https://doi.org/10.1029/](https://doi.org/10.1029/2004JA010649)
 623 [2004JA010649](https://doi.org/10.1029/2004JA010649)
- 624 Kullen, A. (2012). Transpolar arcs: Summary and recent results. *Auroral Phe-*
 625 *nomenology and Magnetospheric Processes: Earth and Other Planets, Geophys.*
 626 *Monogr. Ser.*, *197*, 69–80. doi: <https://doi.org/10.1029/2011GM001183>
- 627 Kullen, A., Brittnacher, M., Cumnock, J., & Blomberg, L. (2002). Solar wind
 628 dependence of the occurrence and motion of polar auroral arcs: A statistical
 629 study. *Journal of Geophysical Research: Space Physics*, *107*(A11), 13–1. doi:
 630 <https://doi.org/10.1029/2002JA009245>
- 631 Lockwood, M., & Cowley, S. (1992). Ionospheric convection and the substorm cycle.

- 632 *Proceedings of the International Conference on Substorms (ICS-1)*, 99–109.
- 633 Marcucci, M., Coco, I., Ambrosino, D., Amata, E., Milan, S., Bavassano Cattaneo,
634 M., & Retinò, A. (2008). Extended SuperDARN and IMAGE observations
635 for northward IMF: Evidence for dual lobe reconnection. *Journal of Geo-*
636 *physical Research: Space Physics*, *113*(A2). doi: [https://doi.org/10.1029/](https://doi.org/10.1029/2007JA012466)
637 [2007JA012466](https://doi.org/10.1029/2007JA012466)
- 638 Milan, S. (2004). A simple model of the flux content of the distant magne-
639 totail. *Journal of Geophysical Research: Space Physics*, *109*(A7). doi:
640 <https://doi.org/10.1029/2004JA010397>
- 641 Milan, S. (2013). Modeling Birkeland currents in the expanding/contracting polar
642 cap paradigm. *Journal of Geophysical Research: Space Physics*, *118*(9), 5532–
643 5542. doi: <https://doi.org/10.1002/jgra.50393>
- 644 Milan, S., Carter, J., Bower, G., Imber, S., Paxton, L., Anderson, B., . . . Hu-
645 bert, B. (2020). Dual-lobe reconnection and horse-collar auroras. *Jour-*
646 *nal of Geophysical Research: Space Physics*, *125*(10), e2020JA028567. doi:
647 <https://doi.org/10.1029/2020JA028567>
- 648 Milan, S., Clausen, L., Coxon, J., Carter, J., Walach, M.-T., Laundal, K., . . . others
649 (2017). Overview of solar wind–magnetosphere–ionosphere–atmosphere cou-
650 pling and the generation of magnetospheric currents. *Space Science Reviews*,
651 *206*(1–4), 547–573. doi: <https://doi.org/10.1007/s11214-017-0333-0>
- 652 Milan, S., Hubert, B., & Grocott, A. (2005). Formation and motion of a transpo-
653 lar arc in response to dayside and nightside reconnection. *Journal of Geo-*
654 *physical Research: Space Physics*, *110*(A1). doi: [https://doi.org/10.1029/](https://doi.org/10.1029/2004JA010835)
655 [2004JA010835](https://doi.org/10.1029/2004JA010835)
- 656 Milan, S., Hutchinson, J., Boakes, P., & Hubert, B. (2009). Influences on the radius
657 of the auroral oval. *Annales Geophysicae*, *27*(7), 2913–2924. doi: [https://doi](https://doi.org/10.5194/angeo-27-2913-2009)
658 [.org/10.5194/angeo-27-2913-2009](https://doi.org/10.5194/angeo-27-2913-2009)
- 659 Milan, S., Lester, M., Cowley, S., & Brittnacher, M. (2000a). Convection and au-
660 roral response to a southward turning of the IMF: Polar UVI, CUTLASS, and
661 IMAGE signatures of transient magnetic flux transfer at the magnetopause.
662 *Journal of Geophysical Research: Space Physics*, *105*(A7), 15741–15755. doi:
663 <https://doi.org/10.1029/2000JA900022>
- 664 Milan, S., Lester, M., Cowley, S., & Brittnacher, M. (2000b). Dayside con-
665 vection and auroral morphology during an interval of northward inter-
666 planetary magnetic field. *Annales Geophysicae*, *18*(4), 436–444. doi:
667 <https://doi.org/10.1007/s00585-000-0436-9>
- 668 Milan, S., Provan, G., & Hubert, B. (2007). Magnetic flux transport in the Dungey
669 cycle: A survey of dayside and nightside reconnection rates. *Journal of Geo-*
670 *physical Research: Space Physics*, *112*(A1). doi: [https://doi.org/10.1029/](https://doi.org/10.1029/2006JA011642)
671 [2006JA011642](https://doi.org/10.1029/2006JA011642)
- 672 Murphree, J., Anger, C., & Cogger, L. (1982). The instantaneous relation-
673 ship between polar cap and oval auroras at times of northward interplan-
674 etary magnetic field. *Canadian Journal of Physics*, *60*(3), 349–356. doi:
675 <https://doi.org/10.1139/p82-047>
- 676 Ness, N., Scarce, C., & Cantarano, S. (1967). Probable observations of the geomag-
677 netic tail at 10^3 Earth radii by Pioneer 7. *Journal of Geophysical Research*,
678 *72*(15), 3769–3776.
- 679 Paxton, L., Meng, C.-I., Fountain, G., Ogorzalek, B., Darlington, E., Gary, S., . . .
680 others (1992). Special sensor ultraviolet spectrographic imager: An instru-
681 ment description. In *Instrumentation for planetary and terrestrial atmospheric*
682 *remote sensing* (Vol. 1745, pp. 2–15). doi: <https://doi.org/10.1117/12.60595>
- 683 Paxton, L., Schaefer, R., Zhang, Y., & Kil, H. (2017). Far ultraviolet instrument
684 technology. *Journal of Geophysical Research: Space Physics*, *122*(2), 2706–
685 2733. doi: <https://doi.org/10.1002/2016JA023578>
- 686 Paxton, L., & Zhang, Y. (2016). Far ultraviolet imaging of the aurora. In *Space*

- 687 *weather fundamentals* (pp. 213–244). CRC Press.
- 688 Paxton, L., Zhang, Y., Kil, H., & Schaefer, R. (2021). Exploring the upper atmo-
689 sphere: Using optical remote sensing. *Upper Atmosphere Dynamics and Ener-*
690 *getics*, 487–522. doi: <https://doi.org/10.1002/9781119815631.ch23>
- 691 Pinnock, M., Rodger, A., Dudeney, J., Rich, F., & Baker, K. (1995). High spa-
692 tial and temporal resolution observations of the ionospheric cusp. *Annales*
693 *Geophysicae*, 13(9), 919–925. doi: <https://doi.org/10.1007/s00585-995-0919-9>
- 694 Provan, G., Yeoman, T. K., & Milan, S. E. (1998). CUTLASS Finland radar
695 observations of the ionospheric signatures of flux transfer events and the
696 resulting plasma flows. *Annales Geophysicae*, 16(11), 1411–1422. doi:
697 <https://doi.org/10.1007/s00585-998-1411-0>
- 698 Reiff, P., & Burch, J. (1985). IMF By-dependent plasma flow and birkeland currents
699 in the dayside magnetosphere: 2. A global model for northward and southward
700 IMF. *Journal of Geophysical Research: Space Physics*, 90(A2), 1595–1609. doi:
701 <https://doi.org/10.1029/JA090iA02p01595>
- 702 Rich, F., & Hairston, M. (1994). Large-scale convection patterns observed by
703 DMSP. *Journal of Geophysical Research: Space Physics*, 99(A3), 3827–3844.
704 doi: <https://doi.org/10.1029/93JA03296>
- 705 Ruohoniemi, J., & Baker, K. (1998). Large-scale imaging of high-latitude convec-
706 tion with Super Dual Auroral Radar Network HF radar observations. *Journal*
707 *of Geophysical Research: Space Physics*, 103(A9), 20797–20811. doi: <https://doi.org/10.1029/98JA01288>
- 709 Siscoe, G. L., Farrugia, C. J., & Sandholt, P. E. (2011). Comparison between the
710 two basic modes of magnetospheric convection. *Journal of Geophysical Re-*
711 *search: Space Physics*, 116(A5). doi: <https://doi.org/10.1029/2010JA015842>
- 712 Song, P., DeZeeuw, D., Gombosi, T., Groth, C., & Powell, K. (1999). A numerical
713 study of solar wind-magnetosphere interaction for northward interplanetary
714 magnetic field. *Journal of Geophysical Research: Space Physics*, 104(A12),
715 28361–28378. doi: <https://doi.org/10.1029/1999JA900378>
- 716 Thomas, E. G., & Shepherd, S. G. (2018). Statistical patterns of ionospheric con-
717 vection derived from mid-latitude, high-latitude, and polar SuperDARN HF
718 radar observations. *Journal of Geophysical Research: Space Physics*, 123(4),
719 3196–3216. doi: <https://doi.org/10.1002/2018JA025280>
- 720 Waters, C., Anderson, B., & Liou, K. (2001). Estimation of global field aligned
721 currents using the Iridium® system magnetometer data. *Geophysical Research*
722 *Letters*, 28(11), 2165–2168. doi: <https://doi.org/10.1029/2000GL012725>
- 723 Wild, J., Cowley, S. W. H., Davies, J., Khan, H., Lester, M., Milan, S., . . . oth-
724 ers (2001). First simultaneous observations of flux transfer events at the
725 high-latitude magnetopause by the Cluster spacecraft and pulsed radar sig-
726 natures in the conjugate ionosphere by the CUTLASS and EISCAT radars.
727 *Annales Geophysicae*, 19(10/12), 1491–1508. doi: [https://doi.org/10.5194/](https://doi.org/10.5194/angeo-19-1491-2001)
728 [angeo-19-1491-2001](https://doi.org/10.5194/angeo-19-1491-2001)
- 729 Woch, J., & Lundin, R. (1992). Magnetosheath plasma precipitation in the polar
730 cusp and its control by the interplanetary magnetic field. *Journal of Geophys-*
731 *ical Research: Space Physics*, 97(A2), 1421–1430. doi: [https://doi.org/10.1029/](https://doi.org/10.1029/91JA02487)
732 [91JA02487](https://doi.org/10.1029/91JA02487)
- 733 Wolfe, J., Silva, R., McKibbin, D., & Mason, R. (1967). Preliminary observations
734 of a geomagnetospheric wake at 1000 Earth radii. *Journal of Geophysical Re-*
735 *search*, 72(17), 4577–4581. doi: <https://doi.org/10.1029/JZ072i017p04577>
- 736 Zhang, Q.-H., Zhang, Y.-L., Wang, C., Lockwood, M., Yang, H.-G., Tang, B.-B.,
737 . . . others (2020). Multiple transpolar auroral arcs reveal insight about
738 coupling processes in the Earth’s magnetotail. *Proceedings of the National*
739 *Academy of Sciences*, 117(28), 16193–16198. doi: [https://doi.org/10.1073/](https://doi.org/10.1073/pnas.2000614117)
740 [pnas.2000614117](https://doi.org/10.1073/pnas.2000614117)
- 741 Zhang, Y., Paxton, L., Zhang, Q.-H., & Xing, Z. (2016). Polar cap arcs: Sun-aligned

742 or cusp-aligned? *Journal of Atmospheric and Solar-Terrestrial Physics*, 146,
743 123–128. doi: <https://doi.org/10.1016/j.jastp.2016.06.001>
744 Zhu, L., Schunk, R., & Sojka, J. (1997). Polar cap arcs: a review. *Journal of At-*
745 *mospheric and Solar-Terrestrial Physics*, 59(10), 1087 - 1126. doi: [https://doi](https://doi.org/10.1016/S1364-6826(96)00113-7)
746 [.org/10.1016/S1364-6826\(96\)00113-7](https://doi.org/10.1016/S1364-6826(96)00113-7)